JOURNAL OF RHEOLOGY

# Constriction flows of monodisperse linear entangled polymers: Multiscale modeling and flow visualization

M. W. Collis, A. K. Lele, M. R. Mackley, R. S. Graham, D. J. Groves et al.

Citation: J. Rheol. **49**, 501 (2005); doi: 10.1122/1.1849180
View online: http://dx.doi.org/10.1122/1.1849180
View Table of Contents: http://www.journalofrheology.org/resource/1/JORHD2/v49/i2
Published by the The Society of Rheology

# Constriction flows of monodisperse linear entangled polymers: Multiscale modeling and flow visualization

M. W. Collis, A. K. Lele, and M. R. Mackley

*Department of Chemical Engineering, University of Cambridge, Pembroke Street, Cambridge CB2 3RA, United Kingdom*

R. S. Graham, D. J. Groves, A. E. Likhtman, and T. M. Nicholson[a)]

*IRC in Polymer Science and Technology, Department of Physics and Astronomy, University of Leeds, Leeds LS2 9JT, United Kingdom*

O. G. Harlen

*IRC in Polymer Science and Technology, Department of Applied Mathematics, University of Leeds, Leeds LS2 9JT, United Kingdom*

T. C. B. McLeish[b)]

*IRC in Polymer Science and Technology, Department of Physics and Astronomy, University of Leeds, Leeds LS2 9JT, United Kingdom*

L. R. Hutchings

*Department of Chemistry, University of Durham, Durham DH1 3LE, United Kingdom*

C. M. Fernyhough and R. N. Young

*Department of Chemistry, University of Sheffield, Sheffield S3 7HF, United Kingdom*

(Received 29 July 2004; final revision received 1 November 2004)

## Synopsis

We explore both the rheology and complex flow behavior of monodisperse polymer melts. Adequate quantities of monodisperse polymer were synthesized in order that both the materials rheology and microprocessing behavior could be established. In parallel, we employ a molecular theory for the polymer rheology that is suitable for comparison with experimental rheometric data and numerical simulation for microprocessing flows. The model is capable of matching both shear

---

[a)]Also at: Division of Chemical Engineering, University of Queensland, Queensland 4072, Australia.
[b)]Author to whom all corresponds should be addressed; electronic mail: t.c.b.mcleish@leeds.ac.uk

and extensional data with minimal parameter fitting. Experimental data for the processing behavior of monodisperse polymers are presented for the first time as flow birefringence and pressure difference data obtained using a Multipass Rheometer with an 11:1 constriction entry and exit flow. Matching of experimental processing data was obtained using the constitutive equation with the Lagrangian numerical solver, FLOWSOLVE. The results show the direct coupling between molecular constitutive response and macroscopic processing behavior, and differentiate flow effects that arise separately from orientation and stretch. © *2005 The Society of Rheology.* [DOI: 10.1122/1.1849180]

## I. INTRODUCTION

A central goal of the polymer rheological community for a number of years has been the connection of polymer melt dynamics at different length scales. The interplay of entropic elasticity and entanglement constraints at the molecular level [Doi and Edwards (1986); McLeish (2002)] led to the subtle and emergent non-Newtonian fluid properties at length scales that average over many molecular interactions. Furthermore, these local fluid properties determine, in principle, the stress and velocity fields in a polymer melt constrained by the complex geometries of processlike flows. Until now, however, there have been few attempts to link molecularly based model calculations across these length scales in the context of experimental data.

Classically, polymer melts have been rheologically characterized, then modeled by parameter fitting one of a family of phenomenological differential or integral constitutive equations [Rajagopalan *et al.* (1993); Baaijens *et al.* (1997)]. This approach suffers from the drawback that models created without reference to molecular physics may fail to represent even qualitative features of the material behavior. This is especially true of long chain branched melts [McLeish and Larson (1999)]. In this case, the recognition that branch points enormously increase the *stretch* relaxation times of polymer chains within their "tubes" produced a new constitutive equation. This approach has been very successful in accounting for the rheology of both model H-shaped monodisperse materials [McLeish and Larson (1999)] and polydisperse melts of low density polyethylene [Verbeeten *et al.* (2001)]. It successfully predicted a qualitatively new feature in the outflow of highly branched melts when coupled to a flow solver [Lee *et al.* (2001)].

Other "micro-macro" approaches have attempted to couple stochastic simulations of the coarse-grained molecular dynamics within the finite elements of a flow simulation [Laso and Öttinger (1993); Peters *et al.* (2000)]. This is, of course, the ideal multilevel approach, but with current levels of computing power, it is not possible to achieve sufficient noise reduction by local ensemble averaging while also addressing the demands of a complex flow field calculation.

Both the molecular constitutive equation and molecular simulation approaches to the problem of multiscale modeling of polymer melts have been constrained by a further problem. The most natural subjects of the model in either case are monodisperse chains that do not require the addressing of complications that arise from the mutual interactions of high and low molecular weight fractions in the distribution. However, although it is possible to synthesize such materials by anionic methods in sufficient quantities for rheological measurements in viscometric flows, the large amounts usually required for complex flow studies have not before been accessible. This is true even for monodisperse linear melts, let alone the more exacting architectures of star, H, and comb molecules [McLeish (2002)].

In this article, we begin to address this missing link by *scaling up* the anionic synthesis of linear melts of polystyrene (PS) and polybutadiene (PB), and simultaneously *scaling down* a representative complex flow. The former will supply quantities of polymer of the

order of tens of grams, rather than grams. The latter, based on the "Multipass Rheometer" of the Cambridge group [Mackley *et al.* (1995)] permits an effectively 4/1 or 11/1 constriction flow. The complex flow, including two sets of re-entrant corners, reversing extensional profile, and transient flow structure, may be analyzed by stress birefringence and pressure difference, but requires only material quantities of this order.

At the same time, we will seek to model the nonlinear rheology and flow properties of this melt by calling on the most recent advances in molecular modeling of entangled polymers. The first versions of the "tube model" dealt restrictively with the two processes of reptation, which diffuses molecules within their entanglement field of tubelike constraints, and retraction, which maintains a constant topological path length for the chains [Doi and Edwards (1986)]. Since then, additional molecular processes have been identified that are essential to a quantitative account of the dynamics of linear entangled chains as probed by both rheology [Likhtman and McLeish (2002a)] and neutron scattering [Wischnewski *et al.* (2002)]. Contour length fluctuation (CLF) permits the extremities of chains to relax faster than the reptation time, while constraint release (CR) links the relaxation of the tube constraint itself to the reptation and CLF of neighboring chains [Likhtman and McLeish (2002)]. In nonlinear deformations, convective CR (CCR) adds to the rate of reconfiguration of the tubes, while stretch suppresses tube reconfiguration and enhances values of stress above the plateau modulus [Mead *et al.* (1998); Ianniruberto and Marrucci (2001)]. This removes the unphysical maximum in shear stress with shear rate that followed from the original approximations of the tube model. Additionally, it permits the prediction of scattering patterns in quantitative agreement with data on strongly sheared entangled melt [Milner *et al.* (2001); Bent *et al.* (2003); Graham *et al.* (2003)]. The level of sophistication, at which all of these molecular processes are presently dealt with in the most detailed accounts of viscometric flows, leads to a level of formalism that would be prohibitive in computations of complex flows. Fortunately, approximations to the full constitutive behavior of models that account for reptation, CLF, CCR, and chain stretch, can be cast in simple, if unfamiliar, forms [Likhtman and Graham (2003)]. This will be the basis of our numerical calculations.

In the next section, we detail the experimental procedures in synthesis and characterization of our materials, the laboratory rheological testing, and the complex flow rheology. In Sec. III, we briefly review the theoretical derivation of the molecular constitutive equations employed to analyze both laboratory viscometric and complex flows. In Sec. IV, we present the experimental phenomena exhibited by monodisperse melts in a constriction flow for the first time, and compare with the model calculations.

## II. EXPERIMENTAL METHOD

### A. Synthesis and characterization

#### *1. Polymerization of butadiene*

The solvents, initiator, and butadiene were purified using standard techniques for anionic polymerization [Morton and Fetters (1975)].

Butadiene was polymerized in *n*-hexane using *sec*-BuLi as the initiator in an all-glass apparatus which had been flamed under a vacuum before use. Reagents were added from ampoules by the rupturing of glass breakseals. Reactions were carried out under a high vacuum at 30 °C for a minimum of 48 h to ensure completion. The reaction was then terminated with methanol.

**TABLE I.** Labels and descriptions of materials used in this study.

| Material label | Description | $M_w$(g/mol) | Polydispersity index |
|---|---|---|---|
| PS260 | Monodisperse PS | 257 800 | 1.03 |
| PS485 | Monodisperse PS | 500 500 | 1.02 |
| PS66 | Monodisperse PS | 67 900 | 1.03 |
| PB48 | Monodisperse PB | 48 100 | 1.01 |
| PB112 | Monodisperse PB | 112 300 | 1.03 |
| PB165 | Monodisperse PB | 165 100 | 1.03 |
| PB210 | Monodisperse PB | 210 500 | 1.04 |

#### *2. Polymerization of styrene*

The synthesis of PS was carried out on a scale of up to 200 g and, as such, involved some modifications to the usual methodology. Polymerizations were carried out in benzene, and purified by passing the solvent sequentially through a column of activated alumina to remove polar impurities and a column of supported copper catalyst to remove traces of oxygen [Pangborn *et al.* (1996)]. Styrene was dried over calcium hydride and degassed by several freeze-thaw cycles. The polymerizations were carried out in a 5 $\ell$ glass reactor, which was evacuated prior to use. After transferring up to 2 $\ell$ of solvent and the monomer to the reactor, any residual impurities were removed by drop-wise addition of the initiator, *sec*-BuLi. Upon the formation of a sustained pale yellow/orange color, attributable to "living" polystyryllithium, the required quantity of initiator was added. All polymerizations were carried out at room temperature and the reactions quenched with degassed methanol. Labels and descriptions of materials used in this study are shown in Table I.

#### *3. Characterization*

Molecular weights were obtained by size exclusion chromatography using a Viscotek 200 with differential refractometer/viscometer/RALLS detectors. Three $(300 \times 7.5$ mm) PLgel 5μ MIXED C columns were used with tetrahydrofuran as the eluent and a flow rate of 1.0 ml/min. The level of 1,4-enchainment of the butadiene was determined by $^1$H nuclear magnetic resonance in $CDCl_3$ at 30 °C using a Bruker AC250MHz spectrometer. For each sample, 93% ($\pm$1%) 1,4-addition was found.

### B. RHEOLOGICAL MEASUREMENTS

#### *1. Sample preparation*

Polymer samples were vacuum dried, compacted using a piston and cylinder as necessary, and then premolded to a suitable thickness and geometry using a template and platen press. Typical molding press temperatures were 90 °C for PB and 180 °C to 200 °C for PS depending on molecular weight. Molding cells with a nitrogen atmosphere or vacuum were available.

#### *2. Shear rheology*

All measurements were made using Rheometrics ARES or RDAII rotational rheometers with a nitrogen atmosphere.

#### 3. Linear rheology

$G(\omega)$ was obtained using time-temperature superposition and a measurement geometry of either 10 mm diameter parallel plates or a 10 mm diameter cone and plate with 2° included angle. PB data were obtained from measurements between −80 °C and 60 °C and PS data between 120 °C and 210 °C.

#### 4. Nonlinear rheology

The relaxation modulus $G(t)$ as a function of strain ($\gamma$) and the transient viscosity $\eta(t)$ as a function of shear rate ($\dot{\gamma}$) were obtained with the cone and plate geometry. The 10 mm diameter and 2° angle were used to reduce large normal forces, when installing the sample and during measurement, and to minimize edge fracture instability [Lee *et al.* (1992); Tanner and Keentok (1983)]. To reduce the tendency for slip at high strains and strain rates, the cone and plate surfaces were grit blasted to produce a surface roughness of approximately 600 grit. Transient viscosity data were corrected for the start time error (strain rate acceleration). At higher strain rates, the transient viscosity was limited to the minimum time and strain to indicate the stress overshoot. This avoided instability allowing repeat measurements on the same test specimen. PB was measured at 20 °C and 50 °C and PS at 170 °C to conform with the elongational data.

#### 5. Elogational rheology

Extensional viscosity was measured in nitrogen using a Rheometrics RME elongational rheometer as described by Meissner and Hostettle (1994). Changes in the rectangular bar specimens, initially 60 mm long with a cross section between 3.5 $mm^2$ and 10.5 $mm^2$ depending on the strain rate and peak force, were monitored during extension by a camera and frame grabber. Corrections were made for true strain rate [Schulze *et al.* (2001)], force base line drift, and start time error. However, the strain rate was determined from change in the sample width due to the need to recover polymer and avoid contamination by particles or markers required for direct extension monitoring. Spacer pins were used between the gripping belts to prevent premature squeeze flow in the sample. There is a narrow temperature window for optimum measurement and the PS was measured at 170 °C.

### C. FLOW VISUALIZATION

The multipass rheometer (MPR) used for the flow visualization experiments was a two-piston capillary-type rheometer developed at the University of Cambridge [Mackley *et al.* (1995)] and is shown schematically in Fig. 1(a). The latest (Mk IV) design has a reduced volume and requires less than a 10 g sample, thereby enabling microprocessing studies to be made on the synthesized monodisperse polymers. The molten polymer was forced backward and forward at controlled piston velocities through an optical flow cell and the flow-induced birefringence technique was used to observe the stress field within the melt. Additional time dependent pressure difference data could also be followed. These techniques have previously been used in combination with an MPR for molten polyethylene [see for example, Lee and Mackley (2001); Lee *et al.* (2001)].

After the system was loaded and sealed, the pistons were used to set a mean pressure and to carry out a series of experiments for a range of wall shear rates, if necessary, over long periods of time with the same small sample. As the system is enclosed, there was no noticeable degradation of the samples with time. For the experiments reported in this article, we used a "multipass steady" shear operation, which was moving the pistons in unison at a constant velocity. For each stroke, the pressure difference develops quickly

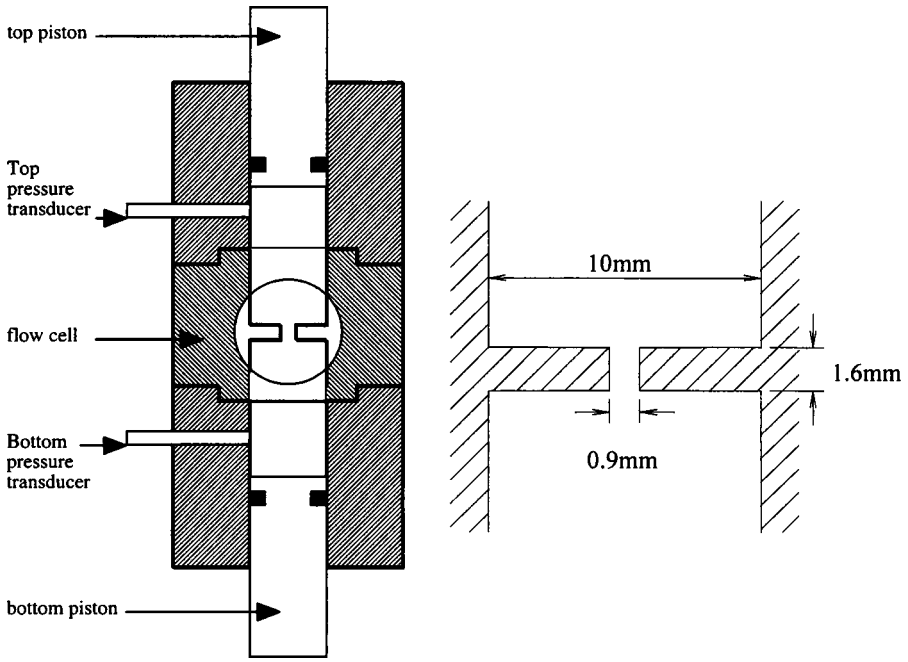


**FIG. 1.** (a) Schematic layout of MPR and (b) cross section of slit flow cell.

across the test section, and for most of the stroke the flow is in a steady state. The general layout of the MPR and test section is shown in Fig. 1. The slit flow cell used was a contraction and expansion flow through a narrow slit, with a cross section as shown in Fig. 1(b); the depth of the cross section was 10 mm and so the channel upstream and downstream of the slit was square. Within the slit the aspect ratio was 11/1 where the flow can approximate to being two dimensional.

For comparison with the inherent relaxation times of the polymers (so determining the regime of non-Newtonian flow), the wall shear rates were estimated both by inverting the Pouseuille expression for the (measured) volume throughput, and by checking against the relevant numerical simulations. The use of flow birefringence is now a well-developed technique for the determination of stress distributions within flowing polymer systems [see for example Baaijens *et al.* (1997)]. The system used here followed that employed by Lee *et al.* (2001). Linearly polarized monochromatic light was passed through quarter-wave plates and received through an analyzer. The observed isochromate fringes then represented integer differences in principal refractive index, which in turn can be expressed as contours of principal stress differences using the stress optical law. In comparison to the cases in which large quantities of commercial material are employed, the quality of the birefringence photographs was not as high, although the geometry and number of fringes were generally clear. This was partly due to the presence of debris material from the synthesis and processing, and the inability to flush the apparatus through with quantities of melt.

## III. THEORY AND MODELING

### A. Tube theory in fast flow

The tube model requires just two parameters for each choice of local polymer chemistry, reflecting the physics at the coarse-grained level of the tube diameter: The entangle-

ment modulus $G_e$, (or alternatively the plateau modulus $G_N^{(0)}$) and the Rouse relaxation time of an entanglement segment $\tau_e$ [McLeish (2002)]. The tube diameter $a$ is not an additional parameter, but is related to $G_e$ via the definition of $M_e$ [Larson *et al.* (2003)]. At 170 °C, we find that these are $2.0\times10^5$ Pa and $7.1\times10^{-4}$ s, respectively, for PS, by fitting the molecular theory of Likhtman and McLeish (2002) to a wide data set. Treating all of the physics in the greatest detail requires solving a partial differential equation for the tensor correlation function $\boldsymbol{f}(s,s';t)$ defined in terms of the arc coordinate of the polymers $\boldsymbol{R}(s,t)$, averaged over chains as

$$f_{\alpha\beta}(s,s';t) \equiv \left\langle \frac{\partial R_\alpha(s,t)}{\partial s}\frac{\partial R_\beta(s',t)}{\partial s'} \right\rangle. \tag{1}$$

Both the viscoelastic stress and the single chain scattering function may be calculated from a knowledge of $\boldsymbol{f}$ (the latter within a Gaussian approximation). The full partial differential equation (PDE) for $\boldsymbol{f}(s,s';t)$ contains terms that arise from advection, reptation, CLF, CR, and retraction [Milner *et al.* (2001); Graham *et al.* (2003)]:

$$\begin{aligned}\frac{\partial}{\partial t}f_{\alpha\beta}(s,s';t) &= \kappa_{\alpha\gamma}f_{\gamma\beta} + f_{\alpha\gamma}\kappa_{\gamma\beta} \\ &+ \frac{1}{3\pi^2 Z\tau_e}\left(\frac{Z}{Z^*(t)}\right)^2\left(\frac{\partial}{\partial s}+\frac{\partial}{\partial s'}\right)D^*(s,s';\lambda(s,s'))\left(\frac{\partial}{\partial s}+\frac{\partial}{\partial s'}\right)f_{\alpha\beta} \\ &+ \frac{3a\nu}{2}\left[\frac{\partial}{\partial s}\frac{1}{\lambda(s)}\frac{\partial}{\partial s}(f_{\alpha\beta}-f^{\mathrm{eq}}_{\alpha\beta}) + \frac{\partial}{\partial s'}\frac{1}{\lambda(s')}\frac{\partial}{\partial s'}(f_{\alpha\beta}-f^{\mathrm{eq}}_{\alpha\beta})\right] \\ &+ \frac{R_s}{2\pi^2\tau_e}\left[\frac{\partial}{\partial s}\left(f_{\alpha\beta}\frac{\partial}{\partial s}\ln\lambda(s)\right) + \frac{\partial}{\partial s'}\left(f_{\alpha\beta}\frac{\partial}{\partial s'}\ln\lambda(s')\right)\right].\end{aligned} \tag{2}$$

In Eq. (2), the first term describes advection by the flow, and the second contains both reptation and CLF (from the effective local diffusion constant $D^*(s,s')$. Here, $Z$ is the equilibrium number of entanglement segments comprising the chain, and $Z^*(t)$ is the time dependent instantaneous value that may differ from $Z$ because of chain stretch. The third term arises from CR, and models the *tube* as a free polymerlike object with a local hopping rate $\nu$. In the language of polymer physics, this is equivalent to a "Rouse theory" of the tube. The dynamics of $\boldsymbol{f}(s,s';t)$ arising from CR alone then take the form of a diffusion equation in the two variables $s$ and $s'$. Here, $a$ is the "tube diameter," related to the plateau modulus directly, $\lambda(s)$ is the local mean stretch of the chains, given by $\lambda(s)=\sqrt{\mathrm{Tr}\, f_{\alpha\beta}(s,s')}$. The CR rate $\nu$ is calculated in turn self-consistently from averages of both reptation (diffusive CR) and retraction (CCR) over the ensemble. The only additional parameter not precisely known at present is the $O(I)$ dimensionless constant that counts the number of local hops of a tube segment generated by one CR event. But comparison of the full theory to date, as well as theoretical considerations of the tube arising as a many-body effect (many chains intersect the volume of a single tube segment), suggests a value for this number, termed $c_\nu$, as $c_\nu=0.1$, which we use in all calculations. For full details, see Graham *et al.* (2003). The final term accounts for free-Rouse chain retraction along its deforming tube. The constant $R_s$ accounts for the decoupling approximation used in the retraction term. Graham *et al.* (2003) demonstrated that a universal value of $R_s=2.0$ produces uniform agreement over a wide range of experimental data and we employ this value for all calculations.

### B. Nonlinear constitutive equation

Although this detailed theory is necessary to make contact with the scattering experiment, it is at present not feasible to use it locally in a finite-element calculation of the flow. Fortunately, calculation of the flow and stress fields requires only a simpler constitutive equation that is able to calculate the stress generated by a given flow history on an element of fluid. Recent work by Likhtman and Graham (2003) has shown that the full treatment at the level of $\boldsymbol{f}(s,s';t)$ may be projected onto a simpler equation for the stress $\sigma_{\alpha\beta}$ only, that preserves the quality of rheological prediction. Based on the "ROuse-CCR tube model for LInear Entangled POLYmers," the "RoliePoly" constitutive equation takes the form

$$\frac{\partial \sigma_{\alpha\beta}}{\partial t} = (\kappa_{\alpha\eta} + \kappa_{\eta\alpha})\sigma_{\eta\beta} - \frac{1}{\tau_d}(\sigma_{\alpha\beta} - \delta_{\alpha\beta}) - \frac{2\left(1 - \sqrt{\frac{3}{\mathrm{Tr}\,\sigma}}\right)}{\tau_R}\left(\sigma_{\alpha\beta} + \beta\left(\frac{\mathrm{Tr}\,\sigma}{3}\right)^{\delta}(\sigma_{\alpha\beta} - \delta_{\alpha\beta})\right). \quad (3)$$

Here, the four terms correspond to: (1) Advection, (2) reptation, (3) chain retraction, and (4) CCR. Likhtman and Graham (2003) found that the parameter values $\beta=1$ and $\delta=-0.5$ gave the closest fit to the predictions of the full model with the preferred CR parameter of $c_\nu=0.1$. The negative value of $\delta$ is instructive: It implies that strong stretching flow suppresses CCR. One physical way in which this might arise is that the longer path length of the stretched molecules simply pick up more entanglements, so that the CCR-generated drag is greater. This is, however, not obvious: An alternative picture might view the entanglement structure simply convecting with chain stretch. The corresponding predictions of the latter are, however, not consistent with transient shear rheology. For a full discussion, see Graham *et al.* (2003). To recover the details of the linear spectrum of our materials, up to six modes carrying the nonlinear structure of Eq. (3) were used to make computable models of the series of monodisperse melts that approximated closely to the rheology of both the material and the full model in the flow rates of the experiment.

### C. Flow computation

The time dependent flow of polymer in the MPR was simulated using the Lagrangian–Eulerian finite-element solver developed at Leeds University [Bishko *et al.* (1999)], using the RoliePoly constitutive model described above. In this method, the fluid velocity at each time step is calculated using a standard *Eulerian* finite-element technique, while the evolution of the stress is calculated in a *Lagrangian* frame by allowing each element to deform with the local velocity gradient. Details of the numerical method are given in Bishko *et al.* (1999).

The flow domain is divided into triangular elements, with velocities and pressures held at the vertices in a continuous interpolation, and material constitutive parameters ($\sigma$ in the RoliePoly equations, which incorporates chain orientation and stretch) piecewise constant on each element. Modes with relaxation rates much faster than the fluid velocity gradients behave as a Newtonian fluid with viscosity $G_i\tau_{bi}$, and so to reduce computational time, modes for which $\dot{\gamma}\tau_{di} \leqslant 0.01$ were treated as Newtonian solvent. Here $\dot{\gamma} = Q/d^2$ is the typical shear rate in the constriction where $Q$ is the area flow rate and $d$ is the width of the channel.

At each time step, the velocity ($\mathbf{u}$) and pressure ($p$) are found from a finite-element solution of the equations of mass and momentum conservation

$$\mu\nabla^2\mathbf{u} - \nabla p = -\nabla \cdot \boldsymbol{\sigma},$$
$$\nabla \cdot \mathbf{u} = 0. \tag{4}$$

Here, $\mu$ is the effective viscosity formed from the short relaxation time modes. The calculated velocities are then used to advect the grid with the flow and the corresponding triangle deformations are used to update the internal constitutive parameters for the triangles. The full RoliePoly equation was used for only the slowest mode, other modes used the nonstretching version of the equations [Likhtman and Graham (2003)]. The vertices are then reconnected as necessary to maintain a *Delaunay* triangulation. The reconnection process introduces a small degree of stress diffusion, but this is controlled by convergence under grid refinement. The resolution of the grid is maintained by an automated adaptive routine which divides any element whose side length is greater than a prescribed maximum length, $\ell_{\max}$ (which is a function of position, so that finer grids may be specified in regions of high gradients).

At the start of the simulation, the entire domain is filled with undeformed fluid, thus the transient effects of start-up flow are simulated. Since the flow domain is symmetric, only one-half of the domain needs to be calculated. In order to reduce the size of the calculation further, a full two-dimensional (2D) model is only employed in the region from two channel widths upstream to two channel widths downstream of the contraction. The region far upstream of the contraction is modeled as start-up flow in a uniform channel using a one-dimensional (1D) simulation employing the same RoliePoly constitutive equations. These velocities are then transferred to vertices in the flow entry region of the 2D simulation. In order to mimic the small, but non-negligible compression of the upstream reservoir, a single-exponential time dependence of growth toward the steady-state upstream velocity was introduced at the upstream boundary (see below). Observation of the results indicates that deviations from uniform channel flow do not start until well into the modeled region. Thus, any upstream effects of the piston in the experimental geometry are not modeled. At the bottom of the simulated region, vertices are removed from the simulation and velocities from the uniform 1D channel flow model are imposed on the flow exit boundary points.

Following previous work [Lee *et al.* (2001)], the convergence of the numerical scheme was tested by using three different levels of mesh refinement in the region near the contraction. A satisfactory degree of convergence was obtained using a mesh that contained approximately ten elements spanning the narrow constriction in the center of the simulation. The stress singularity at the sharp right-angled corners at the entrance to the contraction was avoided by rounding these corners with a radius of 1% of the channel width [Bishko *et al.* (1999)]. Each simulation took approximately 50 h to run on a 633 MHz Pentium III processor.

## IV. RESULTS AND DISCUSSION

### A. Viscometric flows

All the materials were analyzed in linear rheological response and in transient shear, and compared to both the full PDE and RoliePoly constitutive equations. These tube models require just two parameters (plus the weak CCR parameter $\nu$, which we have set to 0.1) for each choice of local polymer chemistry, reflecting the physics at the coarse-grained level of the tube diameter: the entanglement modulus $G_e$ (defined as $5/4$ times

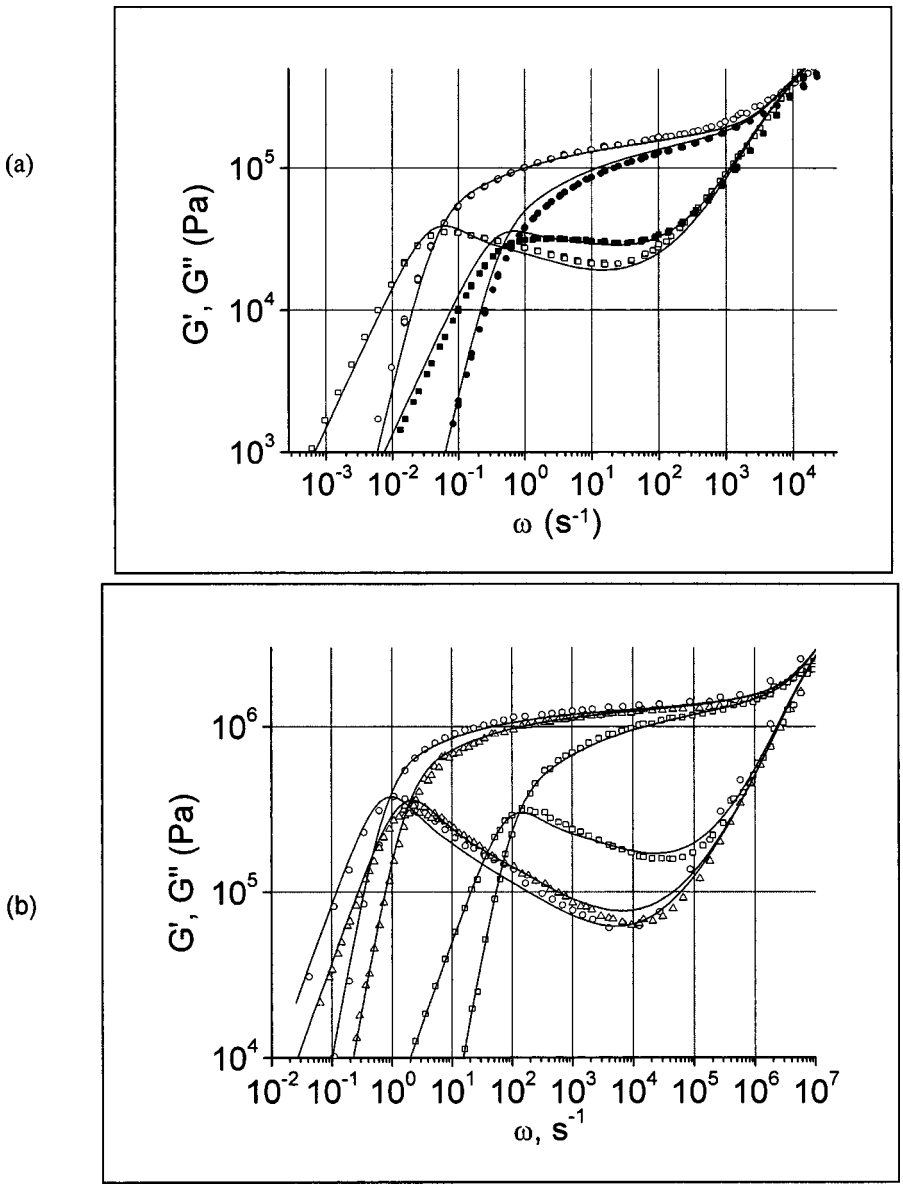


**FIG. 2.** Linear rheology of (a) 250k (filled symbols) and 485k PS (open symbols) melts and (b) PB 48 (squares), 156 (triangles), and 210k (circles) melts with comparison to predictions from the tube theory, parameterized by a chemistry- and temperature-dependent entanglement modulus $G_e$ and Rouse relaxation time of an entanglement segment $\tau_e$, and the material dependent number of entanglements $Z$.

the plateau, modulus $G_N^{(0)}$), and the Rouse relaxation time of an entanglement segment $\tau_e$. For PS at 170 °C, these are $2.04\times10^5$ Pa and $7.1\times10^{-4}$ s, respectively, and for PB at 25 °C they are $1.6\times10^6$ Pa and $4.8\times10^{-7}$ s.

Figure 2 shows the measured linear rheology of representative materials compared with the full tube model in linear response of Likhtman and McLeish (2002). The terminal, reptation time itself, corrected for contour length fluctuations, is calculated in this formulation of the tube theory from the series:

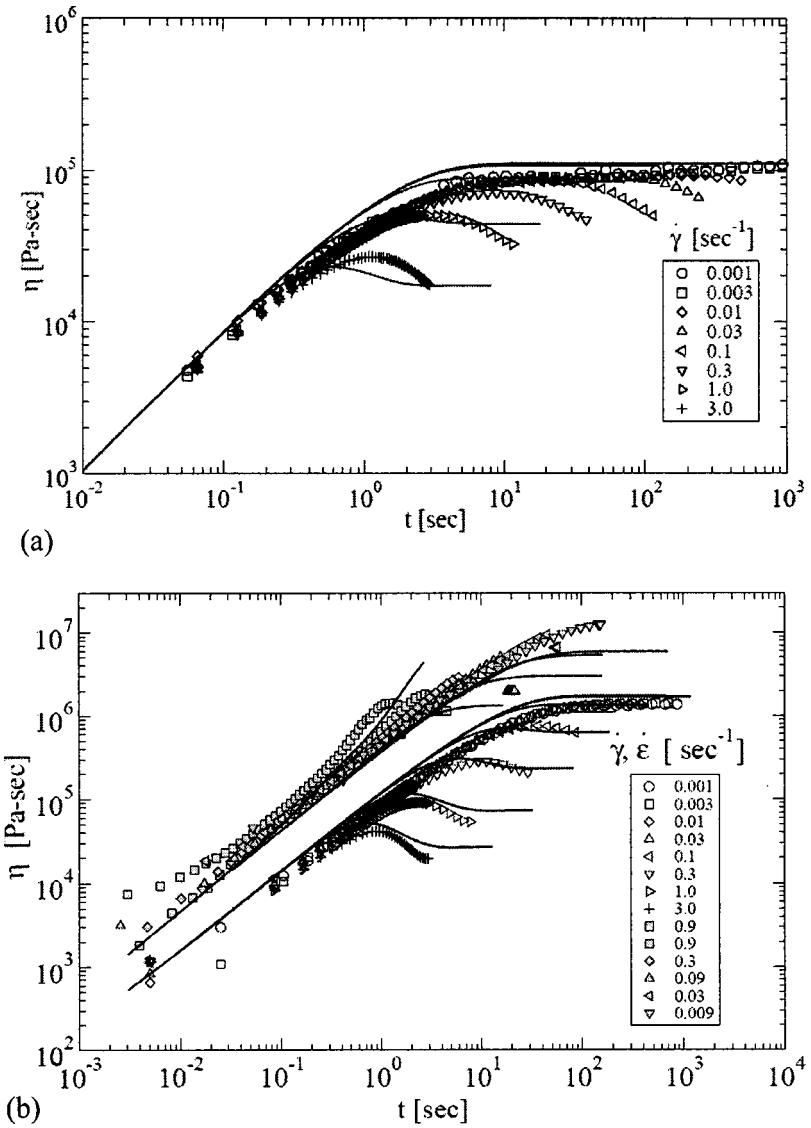


**FIG. 3.** Nonlinear shear and extensional (485k PS only) transients (rates from 0.01–3 $s^{-1}$) rheology of 250k (a) and 485k PS (b) melts at 170 °C (the extensional data were time-temperature shifted from 160 °C). Comparison curves are predictions from the full tube theory of Eq. (2), parameterized by plateau modulus $G_N^{(0)}$, entanglement time $\tau_e$, and the number of entanglements $Z$.

$$\frac{\tau_d(Z)}{\tau_0(Z)} = 1 - \frac{2.38}{Z^{1/2}} + \frac{4.17}{Z} - \frac{1.55}{Z^{3/2}}, \tag{5}$$

where the "bare" reptation time $\tau_0(Z) = 3Z^3\tau_e$. The terminal time, shape of terminal peak, slope of $G''(\omega)$ at higher frequencies, and the minimum are all captured by the theory using a unique parameter set for each chemistry.

Figure 3 contains the transient nonlinear data for two representative PS samples in shear, and the higher molecular weight also in extension. Also given are the predictions for these viscometric flows from the full tube model of Eq. (2), setting the constraint

**TABLE II.** Physical parameters of melt material used in this study.

| | $G_e$(MPa) | $\tau_e$(s) | $M_e$ | $\tau_d$(s) | $\tau_R$(s) | $T$(°C) |
|---|---|---|---|---|---|---|
| PS262 | 0.204 | $7.13\times10^{-4}$ | 17 100 | 2.7 | 0.16 | 170 |
| PS485 | 0.204 | $7.13\times10^{-4}$ | 17 100 | 26.4 | 0.6 | 170 |
| PB48 | 1.6 | $4.8\times10^{-7}$ | 1800 | 0.011 | 0.000 31 | 25 |
| PB165 | 1.6 | $4.8\times10^{-7}$ | 1800 | 0.66 | 0.0037 | 25 |
| PB210 | 1.6 | $4.8\times10^{-7}$ | 1800 | 1.4 | 0.005 | 25 |

release parameter $c_\nu=0.1$. We predict and observe some extensional hardening when the flow rates exceed the Rouse (stretch) relaxation time of the monodisperse linear polymers. The Rouse time may be predicted from molecular theory directly, from

$$\tau_R = Z^2\tau_e, \tag{6}$$

and this value is used within the full tube-CCR model. The Rouse time affects both the shape of the shear transients and the onset and form of the extensional hardening. By this method, we found values of 0.16 s and 0.6 s for PS250 and PS485, respectively, at 170 °C. In particular, in these monodisperse materials with a well-defined lowest Rouse (stretch) relaxation time, the onset of extensional hardening is sudden, as a function of extension rate. This contrasts with commercial materials where the onset is typically much more gradual.

The relaxation times as well as the fixed parameters of the model for the polymers in this study are summarized in Table II. Note that we describe the melt moduli in terms of the parameter $G_e$ of Likhtman and McLeish (2002). It is $5/4$ of a standard values of $G_N^{(0)}$.

The parameters of the RoliePoly equation (amplitude of five modes, reptation, and Rouse times used in the slowest nonlinear mode) were adjusted for each material so that it optimally matched the predictions of the full theory in both extension and in shear. These then became computationally efficient models of the materials to employ in the flow solver. The transient shear flows for the two PS materials matched to the predictions of the RoliePoly models are given in Fig. 4.

### B. Constriction flows

The flow field contains several qualitatively different regions. Slow flow of the Pouseuille type occurs in the broad channels up and downstream. The slot itself is dominated by a much higher wall shear rate, and is preceded by a region of positive extensional deformation upstream, and negative downstream. As we have outlined in Sec. III above, there are *two* important time scales inherent in each of the monodisperse materials we employ: The reptation time $\tau_d$, which determines relaxation of tube segment orientation, and the faster Rouse time $\tau_R$, which determines chain stretch. There are therefore *three* qualitatively different regimes of flow rate, as measured by the wall shear rate in the channel $\dot{\gamma}_w$ (the extension rate at the constriction will be of the same order of magnitude):

(1) $\dot{\gamma}_w\tau_d<1$ linear response;
(2) $\dot{\gamma}_w\tau_d>1, \dot{\gamma}_w\tau_R<1$ orienting flow without chain stretch; and
(3) $\dot{\gamma}_w\tau_d>1, \dot{\gamma}_w\tau_R>1$ orienting flow with chain stretch.

We have been able to fully access the first two regimes experimentally, and to some extent the third (deep into this regime for monodisperse melts results in onset of flow

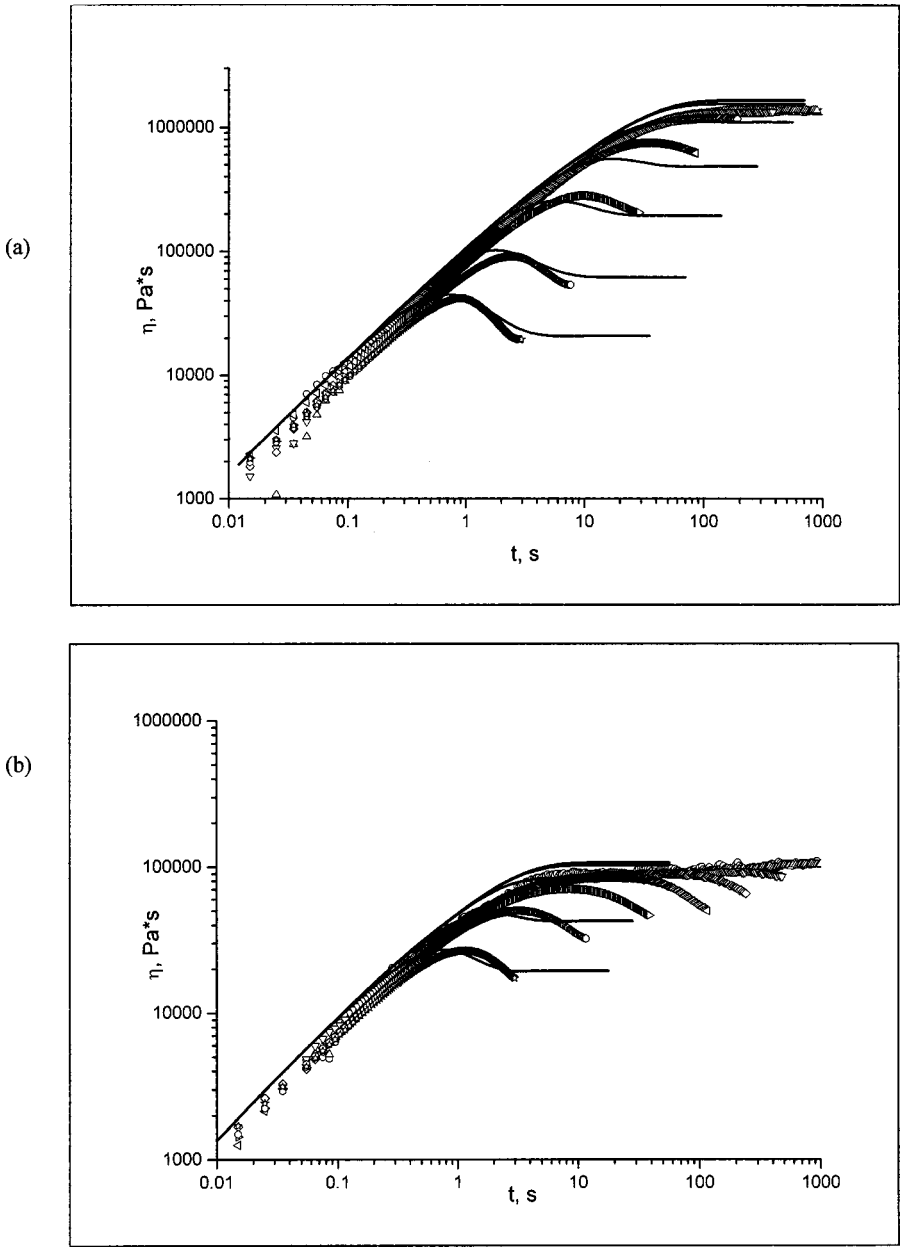


**FIG. 4.** RoliePoly model predictions and comparison to shear transients for (a) PS 262, and (b) PS 485. Strain rates and temperatures are as for Fig. 3.

instabilities). However, all three are accessible computationally, so predictions for Regime (3) will be described in the following. Both PS and PB conform to the universal rheology of the tube model, but differ in that the entanglement molecular weight of PS is much higher than in PB, resulting in less well-entangled melts. The main consequence of this for flow type is that Regime (2) is much broader for the PB samples than for the PS.

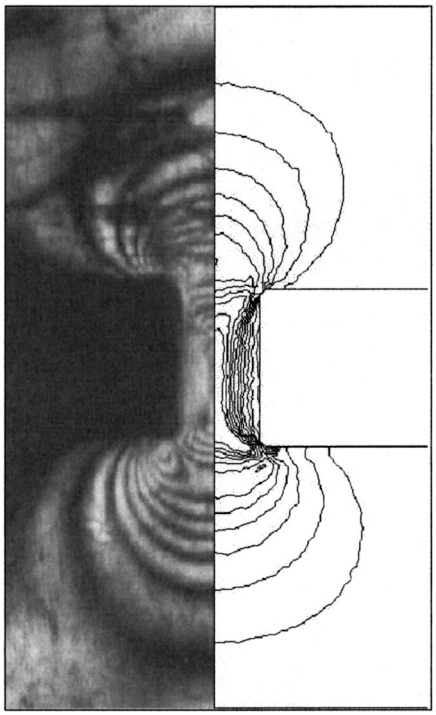

**FIG. 5.** PS 262 at a piston speed of 0.5 mm/s (wall shear rate of 29 $s^{-1}$). The flow is marginally within Regime (3). Observed stress field is on the left, predicted on the right.

### *1. Steady-state flow fields*

We established that the terminal relaxation times of the materials were such that steady states could be achieved at the flow rates employed within a single pass of the MPR pistons. The numerical simulations were also run until a steady state was obtained.

### *2. PS262 melt*

The near symmetry of the observed flow is correctly predicted by the simulations up to the maximum piston speed of 0.5 mm/s (wall shear rate of 29 $s^{-1}$). At this rate, the first asymmetries in the flow, arising from nonlinearities in the material response, can be detected at the outflow. The wall shear rate, made dimensionless by the reptation time is about 80 at this flow rate, but only order 4 with respect to the Rouse time. Stress concentrations arise at the re-entrant corners, and the stress contours away from the die are slightly more linear than in the inflow region.

Figure 5 shows a comparison between the experimentally observed birefringence and the simulated contours of principal stress difference ($\Delta\sigma$). These are related via the stress-optical law:

$$C\Delta\sigma = \frac{k\upsilon}{d}$$

where $\upsilon$ is the wavelength of the light used (514 nm), $d$ is the depth of the sample (10 mm), and $k$ is the fringe number. A value for the stress-optic coefficient, $C$, of 5.6 $\times 10^{-9}$ $Pa^{-1}$ was used for both the PS materials, in agreement with literature values [Janeschitz-Kriegl (1983)]. The immediate finding of both theory and experiment is that,

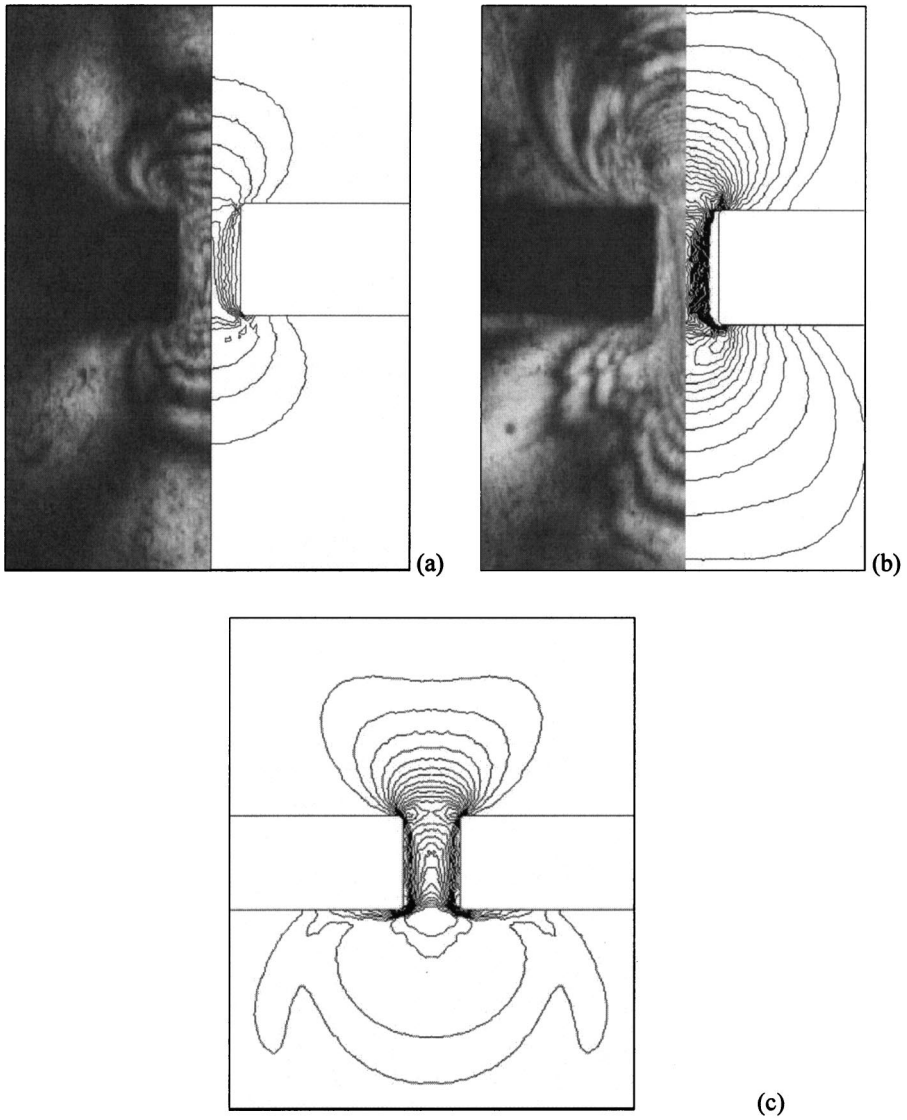


**FIG. 6.** Experiment and calculation of stress fields for the PS485 monodisperse melt. Piston speeds are (a) 0.05 mm/s, (b) 0.2 mm/s, (c) 5 mm/s, giving wall shear rates of (a) 2.9 $s^{-1}$, (b) 12 $s^{-1}$, and (c) 290 $s^{-1}$. Flows (a) is in Regime (2), flow (b) on the threshold of regime (3) and (c) (calculated only) deeply into Regime (3).

although deep into the first nonlinear flow regime, the stress field is highly symmetric, with asymmetry only detected near the corners. Agreement of the predicted and experimental fringe pattern is good.

### *3. PS485 melt*

At lower rates, this higher molecular weight melt, approaching 30 entanglements per chain, exhibits symmetric flows like the less entangled materials. But above piston speeds of (0.05 mm/s, wall shear rate=29 $s^{-1}$) significant asymmetries appeared, leading eventually to unstable flow above 0.2 mm/s. Results of both experiment and simulation are

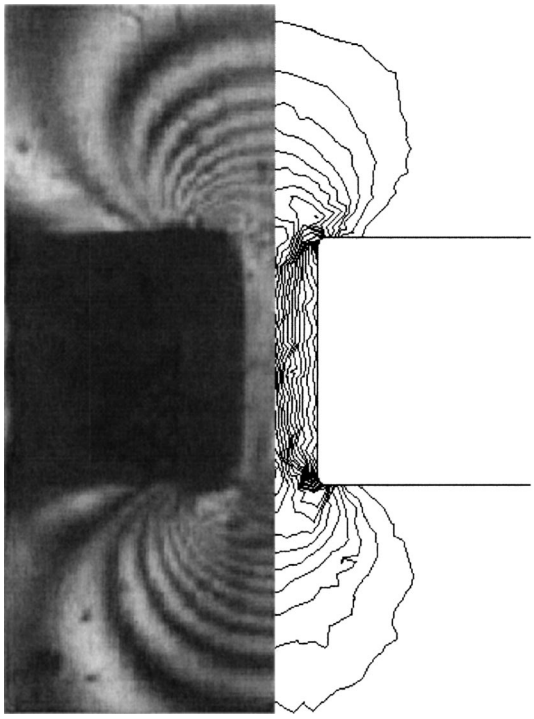

**FIG. 7.** Experimental and simulated stress field from the PB210 melt in the 11:1 contraction at a wall shear rate of 29 $s^{-1}$ at a temperature of 80 °C. The mean dimensionless (by reptation) shear rate is 3.6.

given in Fig. 6. Both the asymmetric stress fields and the instability seem to be hallmarks of the stretching flow Regime (3) of these monodisperse materials. For example, early indications of a three-lobed appearance of the outflow stress region begin to appear at a wall shear rate of 12 $s^{-1}$ [Fig. 6(b)], when $\dot{\gamma}_w \tau_R \cong 7$, and become fully formed at higher rates. These are accessible for this material by simulation only, because the imposition of a symmetry plane along the flow centerline suppresses the instability that occurs in experiment [Fig. 6(c) comes from the simulated steady-state flow at a piston speed of 5 mm/s, far into Regime (3) when $\dot{\gamma}_w \tau_R \cong 40$]. Simulations of the whole channel width (rather than a half-width with imposed symmetry) did indeed show the onset of instabilities above 0.5 mm/s, but this subject will require further study. Yet the simulations at these higher rates are instructive: In Regime (3) the characteristic "fanglike" features of *stretched* material in the outflow, seen hitherto only in transient flows of branched melts [Lee *et al.* (2001)] are predicted to occur even for linear melts. In fact, our calculations predict these features not only in the transient but for steady-state flow as well for monodisperse materials. It will be a challenge to create stable flows in which this prediction can be borne out.

### *4. PB 210k melt*

We may anticipate from studies on the PS material, that the more entangled PB melts are likely to exhibit highly symmetric stress fields in even very nonlinear flows, since the span of Regime (2) for the melts extends to much greater rates. Indeed, at all flow rates accessible experimentally, the flow field was symmetric even though these extend into the first nonlinear Regime (2). We show a representative result for the highest molecular

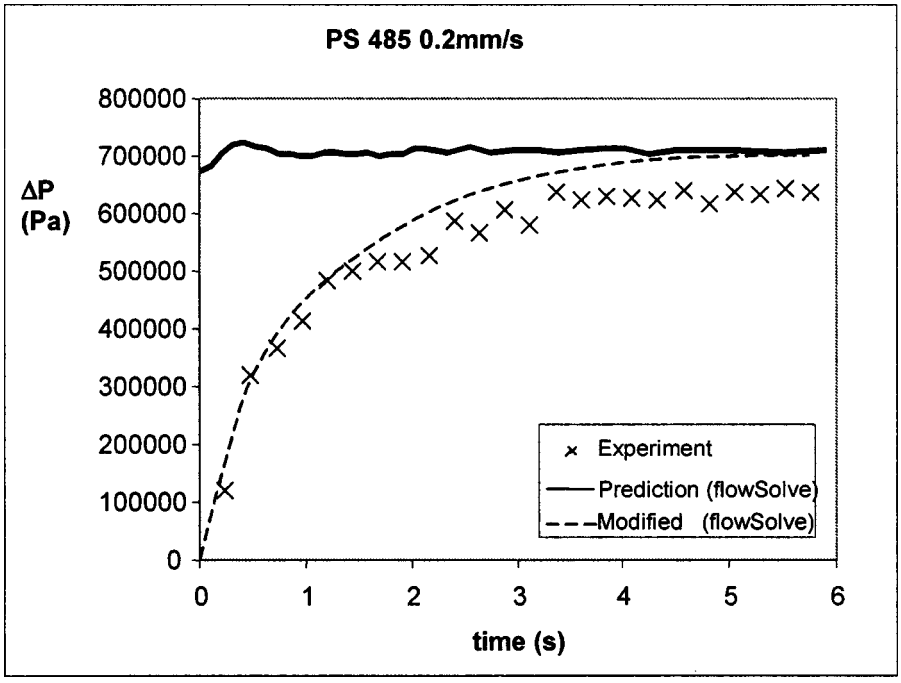


**FIG. 8.** Simulated (solid curve) and experimental data (crosses) on the pressure drop transient for flow start up in an 11:1 contraction of the PS485 melt at 170 °C. The effect of melt compressibility in the upstream piston is marked. The dashed curve shows the modified simulations of the pressure drop when the upstream boundary velocity condition was modulated with a single exponential growth.

weight material PB210 in Fig. 7 when $\dot{\gamma}_w \tau_d \cong 3.6$. The comparison used a stress-optical coefficient of $1.0 \times 10^{-8}$ $Pa^{-1}$, which is rather larger than one literature value of between $2.0 \times 10^{-9}$ $Pa^{-1}$ and $3.0 \times 10^{-9}$ $Pa^{-1}$ [Janeschitz-Kriegl (1983)]. The discrepancy may be related to the far greater tendency for PB to slip in viscometric nonlinear flows than PS. However, both experiment and numerical calculation agree that the only places where any asymmetry is apparent at all (in either experiment or calculation) are the vicinities of the reentrant corners. These are places where, locally, the nonlinearity of the flow is much higher than the mean value.

### *5. Transient flows and pressure drops*

The advantage of both the experimental and numerical protocols we have followed is that fully transient flows may be measured and modeled. Here, we present data on pressure-drop transients, as well as stress-birefringence fields during the flow start up. Naïve comparison of pressure-drop transients lead to a strong disagreement between simulation and experiment: The simulation predicts a very rapid rise of the pressure to a value close to its steady state, yet the experiments show a well-resolved rise time (see Fig. 8). This is due to the compressibility of the upstream reservoir, as shown by a simple calculation. For, in order for the melt to transmit stresses into the constriction of the order of the shear modulus $G_N^{(0)}$, it must be compressed by the piston by relative volume $\Delta V/V$ so that the pressure generated by the bulk modulus $B$ is of order $G_N^{(0)}$:

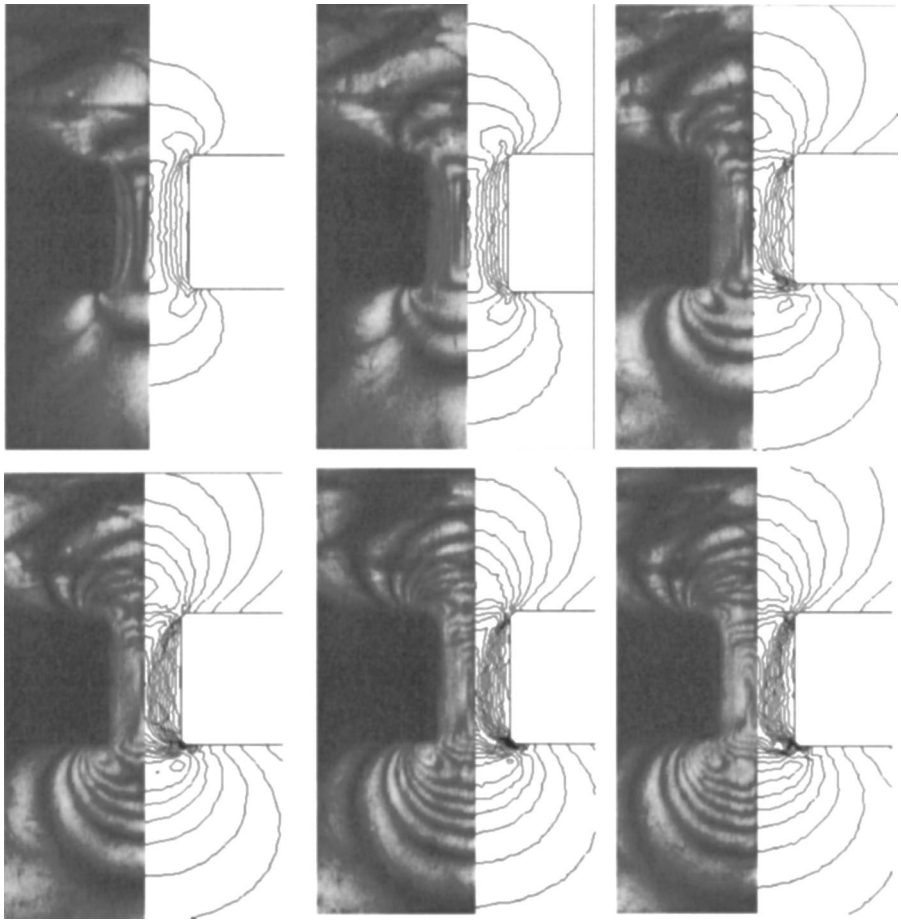

**FIG. 9.** PS262 K at 200 °C—Evolution of flow birefringence at piston speed of 0.5 mm/s (steady-state wall shear rate of 29 $s^{-1}$): (a) $t=0.25$ s, (b) $t=0.5$ s, (c) $t=0.75$ s, (d) $t=1.0$ s, (e) $t=1.25$ s, and (f) $t=1.5$ s (fully developed).

$$B\frac{\Delta V}{V} \cong G_N^{(0)} \tag{7}$$

But, for PS, $B/G_N^{(0)} \sim 10^3$, and, since the upstream piston length is 10 cm, the piston displacement corresponding to this compression is of the order of 0.1 mm. At a piston speed of 0.2 mm/s (that of Fig. 8), the time scale for achieving the steady-state flow at the constriction end of the reservoir is therefore about 0.5 s, as seen in the experiment. We also observe by comparing the characteristic transient time scales with different piston speeds that they follow a constant *bulk strain* of the upstream melt, as predicted by Eq. (6), rather than any constant intrinsic time scale.

In order to permit a realistic comparison of transients from experiment and simulation, the compressibility effect must be accounted for. Simulation of the entire upstream reservoir is unfeasible, so instead we modulate the 1D upstream velocity boundary condition with an exponential decay onto the steady-state value that matches just the time constant of the observed pressure transient (dashed curve in Fig. 8). Under such time dependent forcing, the full stress field in time may be computed and compared to the observed field.

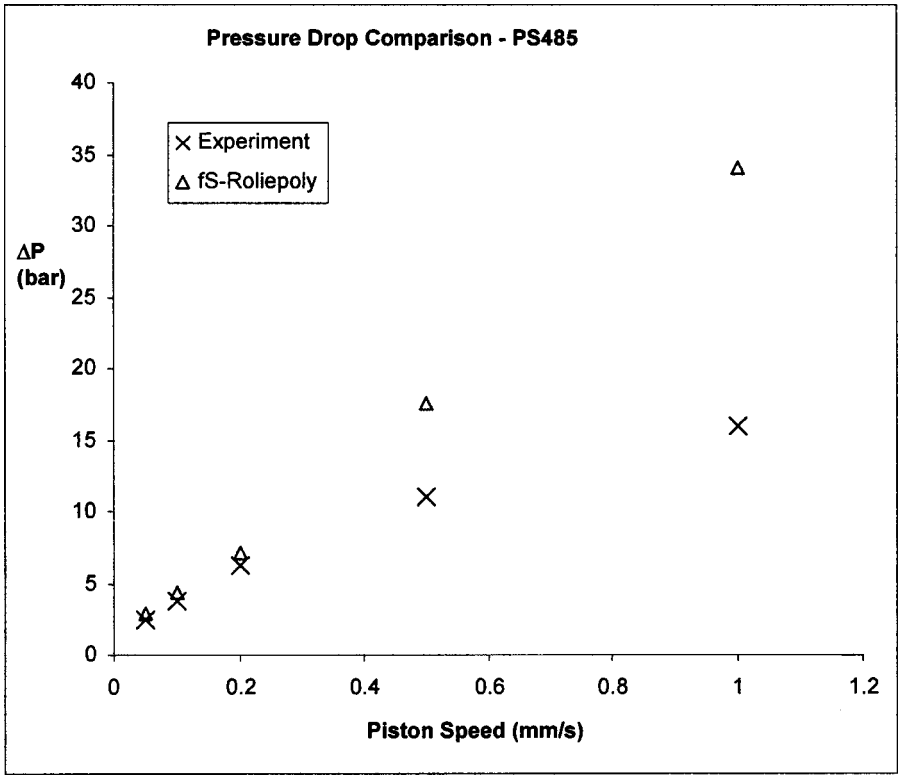


**FIG. 10.** Observed and simulated steady-state pressure drops as a function of piston speed for the PS485 melt. Above 0.5 mm/s (wall shear rate of 29 $s^{-1}$), the observed values fall markedly below the predicted values, but this is also the regime in which the experiment showed flow instabilities, which are suppressed in the simulations.

A series of results is shown in Fig. 9 for the PS262 melt in Regime (2). The overall shape and magnitude of the stress field is captured throughout the transient flow. Furthermore, there are detailed features of the transient flow that are *not* present in the steady flow that appear in both the experiment and simulation. In particular, lobes of high principal stress from the upstream and downstream re-entrant corners grow, then retreat, during the transient. In spite of the allowance for the delay in flow at the constriction itself, however, these features still occur slightly earlier in the simulation than in experiment. For example, the lobe at the upstream re-entrant corner attains maximum extent in the experiment at 1.2 s, while the simulations find this maximum at 0.5 s after start up of flow. This is unlikely to be a constitutive flaw simply related to the viscometric transient response, since the shear overshoots in viscometric flows are well captured by the RoliePoly model.

Figure 10 shows the comparison of predicted and steady-state pressure drops for the high molecular weight PS485 material. The agreement is good well into Regime (2) of nonlinear flow, but as the experiments become increasingly unstable (while the simulations remain artificially stable), an increasingly large overprediction of the stress is observed. This observation of reduction in expected dissipation suggests that the manifestly unstable flow [Fig. 6(b) is a snapshot of an unsteady flow] may also be accompanied by wall slip. This is also consistent with, but not conclusively determined by, the time dependent birefringence images.

## V. CONCLUSIONS

Monodisperse polymer melts clarify rheology in complex flows in a similar way to that in viscometry. In simple rheological response, sharp monodispersity in molecular structure gives rise to a clear "reptation" peak in the loss modulus, and sharp stress overshoots in strong shear transients. These features are universal among entangled polymers when compared at equal degrees of entanglement and entanglement time scale. The corresponding features in the complex constriction flow described here include the highly symmetric stress fields seen in all nonstretching flows, even highly nonlinear ones, and the appearance of very characteristic features in both inflow and outflow when chains become stretched. The advantage of monodispersity at the molecular level is then understood as the separation of time scales for orientation relaxation (reptation) and stretch relaxation (Rouse), and the absence of the mixed states of chains that will naturally arise in a polydisperse blend. Some of these features occur only in the transient flow and not in steady state. The tube model constitutive equation captures these quantitatively, but the *time* at which they occur in the transient is affected (initially surprisingly) by upstream compressibility of the melt reservoir. Simulations that treat only isolated portions of the flow need to be presented with time-modified boundary conditions to correspond to real experiments.

The second advantage (for a scientific study, not for a real process) of very narrow polydispersity is the amplification of flow instabilities that break lateral symmetry. Both experiment and simulation indicate that strongly nonlinear flows are prone, especially in the outflows, to oscillations that direct the centerline alternately to one side, then the other, at a frequency that is set by the characteristic deformation rate in the channel.

## ACKNOWLEDGMENTS

The authors gratefully acknowledge the support of EPSRC (UK) under the "Microscale Polymer Processing" consortium grant, and the essential additional support of BP Chemicals, DuPont Films, DuPont Teijin, Dow Chemical, BASF, DSM, and Lucite International. Helpful discussions with Nat Inkson, Ralph Colby, and Daniel Read assisted the preparation of the manuscript, as did helpful comments from referees.

## References

Baaijens F. P. T., S. H. A. Seelen, H. P. W. Baaijens, G. W. M. Peters, and H. E. H. Meijer, "Viscoelastic flow past a confined cylinder of a low density polyethylene melt," J. Non-Newtonian Fluid Mech. **68**, 173–203 (1997).

Bent J., L. R. Hutchings, R. W. Richards, T. Gough, R. Spares, P. D. Coates, I. Grillo, O. G. Harlen, D. J. Read, R. S. Graham, A. E. Likhtman, D. J. Groves, T. M. Nicholson, and T. C. B. McLeish, "Neutron-mapping polymer flow: Scattering, flow visualization, and molecular theory," Science **301**, 1691–1695 (2003).

Bishko G. B., O. G. Harlen, T. M. Nicholson, and T. C. B. McLeish, "Numerical simulation of the transient flow of branched polymer melts through a planar contraction using the 'pom-pom' Model," J. Non-Newtonian Fluid Mech. **82**, 255–273 (1999).

Doi, M., and S. F. Edwards, *The Theory of Polymer Dynamics* (Oxford University Press, Oxford, UK, 1986).

Graham, R. S., A. E. Likhtman, S. T. Milner, and T. C. B. McLeish, "Microscopic theory of linear entangled polymer chains under rapid deformation including chain stretch and convective constraint release," J. Rheol. **47**, 1171–1200 (2003).

Ianniruberto, G., and G. Marrucci, "A simple constitutive equation for entangled polymers with chain stretch," J. Rheol. **45**, 1305–1318 (2001).

Janeschitz-Kriegl, H., *Polymer Melt Rheology and Flow Birefringence* (Springer, New York, 1983).

Larson, R. G., T. Sridhar, L. G. Leal, G. H. McKinley, A. E. Likhtman, and T. C. B. McLeish, "Definitions of entanglement spacing and time constants in the tube model," J. Rheol. **47**, 809–818 (2003).

Laso, M., and H. C. Öttinger, "Calculation of viscoelastic flow using molecular models: The CONFFESSIT approach," J. Non-Newtonian Fluid Mech. **47**, 1–20 (1993).

Lee, C. S., B. C. Tripp, and J. J. Magda, "Does N1 or N2 control the onset of edge fracture?" J. Rheol. **31**, 306–308 (1992).

Lee, K., and M. R. Mackley, "The application of the multipass rheometer for precise rheooptic characterisation of polyethylene melts," Chem. Eng. Sci. **56**, 5653–5661 (2001).

Lee, K., M. R. Mackley, T. C. B. McLeish, T. M. Nicholson, and O. G. Harlen, "Experimental observation and numerical simulation of transient stress fangs within flowin molten polyethylene," J. Rheol. **45**, 1261–1277 (2001).

Likhtman, A. E., and T. C. B. McLeish, "Quantitative theory for linear dynamics of linear entangled polymers," Macromolecules **35**, 6332–6343 (2002).

Likhtman, A. E., and R. S. Graham, "Simple constitutive equation for linear polymer melts derived from molecular theory: Rolie-Poly equation," J. Non-Newtonian Fluid Mech. **114**, 1–12 (2003).

Mackley, M. R., Marshall, R. T. J., and Smeulders, J. B. A. F., "The multipass rheometer," J. Rheol. **39**, 1293–1309 (1995).

McLeish, T. C. B., "Tube theory of entangled polymer dynamics," Adv. Phys. **51**, 1379–1527 (2002).

McLeish, T. C. B., and S. T. Milner, "Entangled dynamics and melt flow of branched polymers," Adv. Polym. Sci. **143**, 195–256 (1999).

Mead, D. W., R. G. Larson, and M. Doi, "A molecular theory of fast flows of linear polymers," Macromolecules **31**, 7895–7914 (1998).

Meissner J., and J Hostettler, "A new elongational rheometer for polymer melts and other highly viscoelastic liquids," Rheol. Acta **33**, 1–21 (1994).

Milner, S. T., T. C. B. McLeish, and A. E. Likhtman, "Microscopic theory of convective constraint release," J. Rheol. **45**, 539–563 (2001).

Morton, M., and Fetters, L. J., "Anionic polymerization of vinyl monomers," Rubber Chem. Technol. **48**, 359–409 (1975).

Pangborn, A. B., M. A. Giardello, R. H. Grubbs, R. K. Rosen, and F. J. Timmers, "Safe and convenient procedure for solvent purification," Organometallics **15**, 1518–1520 (1996).

Peters, E. A. J. F., A. P. G. van Heel, M. A. Hulsen, and B. H. A. A. van den Brule, "Generalization of the deformation field method to simulate advanced reptation models in complex flow," J. Rheol. **44**, 811–829 (2000).

Rajagopalan, D., R. C. Armstrong, and R. A. Brown, "Comparison of computational efficiency of flow simulations with multimode constitutive equations: Integral and differential models," J. Non-Newtonian Fluid Mech. **46**, 243–273 (1993).

Schulze, J. S., T. P. Lodge, C. W. Macosko, J. Hepperle, H. Munstedt, H. Bastian, D. Ferri, D. J. Groves, Y. H. Kim, M. Lyon, T. Schweizer, T. Virkler, E. Wassner, and W. Zoetelief, "A comparison of extensional viscosity measurements from various RME rheometers," Rheol. Acta **40**, 457–466 (2001).

Tanner R. I., and M. Keentok, "Shear fracture in cone-plate rheometry," J. Rheol. **27**, 47–57 (1983).

Verbeeten, W., G. W. M. Peters, and F. P. T. Baaijens, "The extended pom-pom model," J. Rheol. **45**, 823–843 (2001).

Wischnewski A., M. Monkenbusch, L. Willner, D. Richter, A. E. Likhtman, T. C. B. McLeish, and B. Farago, "Molecular observation of contour-length fluctuations limiting topological confinement in polymer melts," Phys. Rev. Lett. **88**, 058301 (2002).